

~~CONFIDENTIAL~~

6

Copy  
RM E55119

NACA RM E55119

NACA

# RESEARCH MEMORANDUM

PERFORMANCE OF A HIGH-SOLIDITY HIGH-PRESSURE-RATIO

TRANSONIC ROTOR

By Harvey E. Neumann

Lewis Flight Propulsion Laboratory  
Cleveland, Ohio

CLASSIFICATION CHANGED

UNCLASSIFIED

By authority of

*Wash DC - 1*  
*Effective*

Date *9-17-58*

CLASSIFIED DOCUMENT

This material contains information affecting the National Defense of the United States within the meaning of the espionage laws, Title 18, U.S.C., Secs. 793 and 794, the transmission or revelation of which in any manner to an unauthorized person is prohibited by law.

NATIONAL ADVISORY COMMITTEE  
FOR AERONAUTICS

WASHINGTON

November 8, 1955

~~CONFIDENTIAL~~

UNCLASSIFIED



## NATIONAL ADVISORY COMMITTEE FOR AERONAUTICS

RESEARCH MEMORANDUM

## PERFORMANCE OF A HIGH-SOLIDITY HIGH-PRESSURE-RATIO TRANSONIC ROTOR

By Harvey E. Neumann

## SUMMARY


A 14-inch high-solidity mixed-flow transonic rotor with an inlet radius ratio of 0.52 was tested in Freon-12. The rotor developed a total-pressure ratio of 1.93 and an efficiency of 92 percent at an equivalent wheel tip speed of 1036 feet per second in air and an equivalent weight-flow rate of 24.3 pounds per second per square foot frontal area in air. The maximum efficiencies at all lower speeds tested remained above 90 percent. As the weight flow was reduced, an abrupt total-span rotating stall was developed. The stalled region covered approximately one-third of the annulus area. The stall-free range of this rotor is smaller than that of a transonic stage of conventional solidity.

## INTRODUCTION

As shown by engine tests and analyses (refs. 1 and 2), two important off-design axial-flow compressor operating problems are blade failures at low compressor speeds and poor engine acceleration characteristics. These problems result from compressor rotating-stall and surge characteristics. At low compressor speeds the rotating stall is initiated in the inlet stages of the compressor. The blade failures at low compressor speeds are usually due to resonant blade vibrations that arise from the alternate high- and low-flow zones that rotate about the compressor axis during this stalled operation.

During rapid engine acceleration, the turbine-inlet temperature rises and results in lower air flows and higher compressor pressure ratios, thus causing the inlet stages of the compressor to operate closer to the compressor stall-limit line. Poor engine acceleration characteristics can result, therefore, when the inlet stages have an inadequate range of weight flow between the equilibrium operating line and the compressor stall-limit line.

Cascade tests (ref. 3) indicate that wider ranges of weight flow with stable operation can be obtained by increasing the solidity of the



3737

CB-1

blades. In addition, blades with low aspect ratios are less susceptible to resonant blade vibrations induced by rotating stall. The purpose of this investigation was to determine the performance and suitability of a high-solidity low-aspect-ratio transonic rotor for the inlet stages of an axial-flow compressor.

The over-all performance, the evaluation of the weight-flow range, and the associated stator problems of the high-solidity low-aspect-ratio transonic rotor used in this investigation are presented for seven corrected wheel tip speeds from 518 to 1184 feet per second in air. The stall characteristics of the rotor are presented for six corrected wheel tip speeds from 518 to 1036 feet per second in air.

#### SYMBOLS

$\Delta H$	increase in specific stagnation enthalpy from station 0 to station 3, Btu/lb
$\Delta H_{1s}$	increase in specific stagnation enthalpy at constant entropy from conditions at station 0 to $P_3$ , Btu/lb
$i$	angle of incidence, deg
$M$	absolute Mach number, ratio of absolute velocity of fluid to local velocity of sound
$M'$	relative Mach number, ratio of velocity of fluid relative to rotor to local velocity of sound
$P$	absolute total pressure
$P_c$	absolute static pressure on casing
$r$	radial distance from axis of rotation, in.
$U$	rotative speed of rotor, ft/sec
$w$	weight flow of gas, lb/sec
$z$	distance parallel to axis of rotor, in.
$\delta$	ratio of total pressure to standard NACA sea-level pressure
$\epsilon$	angle between axis of rotation and absolute velocity vector, deg
$\eta_{ad}$	adiabatic efficiency of rotor, $\Delta H_{1s}/\Delta H$
$\theta$	ratio of total temperature to standard NACA sea-level temperature

## Subscripts:

- d design
- e equivalent value for standard pressure and temperature
- 0 entrance tank upstream of nozzle (see fig. 1)
- 1 station 1 at rotor entrance (see fig. 1)
- 2 discharge flow conditions from second transonic stage or from assumed stator for high-solidity transonic rotor
- 3 station 3 at rotor exit (see fig. 1)

## ROTOR DESIGN

The rotor tested is a modification of the supersonic rotor with high-solidity blades previously reported in reference 4. The 14-inch-diameter rotor has an inlet radius ratio of 0.52 and 22 aluminum blades of constant thickness (1/8 in.) at the tip.

The rotor of reference 4 employed inlet guide vanes which turned the gas in a direction counter to the wheel rotation. The relative discharge flow of the rotor was turned past axial. With this type of design, the work input decreases with a decrease in flow. Surge analyses (ref. 5) indicate that a wider range of weight flows before encountering surge might be obtained with a design which increases the work input with a decrease in flow. In order to obtain such a characteristic, the inlet guide vanes of the rotor of reference 4 were removed, and the axial length of the rotor was reduced until there was no longer a turning of the flow past axial. The trailing edge was then swept forward at an angle of  $35.93^\circ$  to reduce the radial variation of the work output. A  $15^\circ$  trailing-edge wedge was used. The blade entrance and discharge angles and a schematic diagram of the alteration are given in figure 1. The coordinates of the blade surface and the hub contour are given in reference 4.

The removal of the guide vanes also reduced the inlet Mach number, thus making the inlet conditions more comparable with those of typical transonic inlet stages.

## TEST APPARATUS

The rotor was tested with Freon-12 as the working fluid in a closed system as is shown in figure 2(a). The rotor was driven by a 3000-horsepower variable-frequency motor through a gear train. The pressure

developed by the rotor was dissipated across the discharge throttle at the end of the radial diffuser (fig. 2(b)). The gas flowed from the discharge collector through twin cooler assemblies to the inlet tank. An additional throttle was used in the inlet to control the pressure on the coolers.

#### INSTRUMENTATION AND PROCEDURE

Inlet total pressures and temperatures were measured in the inlet tank, and the weight flow was determined by using the four static-pressure taps of the calibrated nozzle. The test section and the measuring stations are shown in figure 2(b). Total pressures and flow angles at station 1 were determined by 11-point radial surveys using claw - total-pressure probes at three circumferential positions. The static pressures were obtained from four pressure taps on the hub and four on the casing. The variations of the discharge-flow properties were determined at station 3 by radial surveys with four semishielded thermocouple probes, three claw - total-pressure probes, and three L static-pressure probes. The unsteady flow was qualitatively studied with radial surveys using hot-wire anemometers at six circumferential locations at both stations 1 and 3. Five catenary diaphragm pressure transducers were also used to study the unsteady static-pressure fluctuations. Two transducers were placed at station 1 and three at station 3 in circumferential positions such that the number and direction of rotation of rotating phenomena could be determined. The probes and transducer used in this investigation are shown in figure 3. The frequency response of the transducer system was within  $\pm 1$  percent from 0 to 20,000 cps. The resonant frequency of the transducer is approximately 45,000 cps.

The shape of the over-all performance characteristic curves was obtained by measurements at the area centers of three equal annular areas. At certain points of interest more detailed performance was determined by means of 11-point radial surveys.

The performance of this rotor was determined over a range of back pressures from open throttle to nearly closed throttle for six speeds from corrected wheel tip speeds of 518 to 1036 feet per second in air. At a wheel tip speed of 1184 feet per second the performance was determined from open throttle to the incipient-stall point. The inlet-tank pressure varied from 19 to 29 inches of mercury absolute. The inlet total temperature varied from 65° to 110° F. The Freon-12 purity was maintained above 97 percent at all times.

There is an uncertainty of  $\pm 1.5$  percent associated with the adiabatic efficiencies at wheel tip speeds of less than 1036 feet per second due to experimental errors in measuring small temperature rises and pressure

ratios. For a wheel tip speed of 1036 feet per second, calculation of the weight flow from the exit survey gave a value of 22.6 pounds per second per square foot frontal area, whereas the value from the calibrated nozzle was 22.3 pounds per second per square foot frontal area, a difference of 1.3 percent.

## RESULTS AND DISCUSSION

### Over-All Performance

Stall-free performance. - The over-all performance of the rotor in terms of equivalent weight flow, total-pressure ratio, and adiabatic efficiency is shown in figure 4. The peak efficiency (survey data point) at a wheel tip speed of 1036 feet per second was 92 percent at an equivalent weight flow of 24.3 pounds per second per square foot frontal area in air and a total-pressure ratio of 1.93. The maximum flow for a wheel tip speed of 1036 feet per second was 25.6 pounds per second per square foot frontal area in air. When the speed was increased to 1184 feet per second, the peak efficiency decreased to a value of 86 percent at an equivalent weight flow of 25.4 pounds per second per square foot frontal area in air at a total-pressure ratio of 2.34. The maximum flow for a wheel tip speed of 1184 feet per second was 27.5 pounds per second per square foot frontal area in air. When the speed was reduced to wheel tip speeds less than 1036 feet per second, the peak adiabatic efficiency remained above 90 percent. The maximum flows indicated in figure 4 for low wheel speeds represent a limit imposed by the test rig and are not the choking of the flow in the rotor.

Performance during stalled operation. - The stall-limit line, as shown in figure 4(a), is the locus of incipient-stall points. At a wheel tip speed of 1036 feet per second, the incipient-stall point occurs at a flow of 22.2 pounds per second per square foot frontal area in air, an efficiency of 89 percent, and a total-pressure ratio of 1.92. At a wheel tip speed of 1184 feet per second, the incipient-stall point is also the maximum-efficiency operating point.

When the flow is reduced to a value less than the value at the incipient-stall points, a rotating stall develops and causes a discontinuous change in the performance characteristic (fig. 4). Because of this discontinuity in the performance characteristic curve, this type of stall is called "abrupt". If the flow is allowed to increase after obtaining the abrupt stall, the rotor recovers from rotating stall at a greater value of equivalent weight flow than that at the incipient-stall point, thus giving the overlapping of the two branches of the constant-speed performance characteristic curve (fig. 4(a)).

During stalled operation the rotor efficiency was low. At a wheel tip speed of 1036 feet per second, the adiabatic efficiency was 80 percent at an equivalent weight flow of 20.2 pounds per second per square foot frontal area in air and a total-pressure ratio of 1.79. As the flow was further reduced while operating at a wheel speed of 1036 feet per second, the adiabatic efficiency and total-pressure ratio decreased. At all other speeds where stall data were taken, the adiabatic efficiencies were low, and the total-pressure ratio and efficiency both decreased rapidly with a decrease in flow.

#### Inlet Flow

The radial variations in relative inlet Mach number and incidence angle are shown in figures 5(a) and (b), respectively. At all speeds, the relative inlet Mach number (fig. 5(a)) is higher at the tip than the hub. At a wheel tip speed of 1036 feet per second, the relative inlet Mach number at maximum-efficiency operation was 1.05 near the tip and 0.66 near the hub. This range of inlet Mach numbers is typical for current transonic rotors when operating at design wheel tip speeds of approximately 1000 feet per second.

When the flow is reduced while operating at a constant speed, the relative inlet Mach number remains approximately constant, whereas the incidence angle increases (fig. 5(b)). At a wheel tip speed of 1036 feet per second, the relative inlet Mach number near the tip (a radius of 6.66 in.) varies from 1.05 to 0.99, whereas the incidence angle (at the same radius) varies from  $0.4^\circ$  to  $5.1^\circ$  for the entire stall-free range of weight flows. The incidence angle near the hub is smaller than the value near the tip, although the range of incidence angle from the maximum-flow point to the incipient-stall point remains approximately the same at all radii. At a wheel tip speed of 1036 feet per second, the incidence angle near the hub (a radius of 3.85 in.) is  $-5.2^\circ$  at the maximum-flow point and  $0.5^\circ$  at the incipient-stall point. As the speed is increased while operating at incipient-stall points, the incidence angle decreases. Near the mean radius (a radius of 5.05 in.) the incidence angle is  $7.8^\circ$  for a wheel tip speed of 518 feet per second and  $4.0^\circ$  for a wheel tip speed of 1036 feet per second.

#### Exit Flow

The radial variations of absolute discharge Mach number, absolute discharge angle, and total-pressure ratio are given in figures 6(a), (b), and (c), respectively, for the maximum weight flow, maximum efficiency, and incipient-stall points. The radial variation of absolute discharge Mach number (fig. 6(a)) is small at all speeds tested except

at a wheel tip speed of 1184 feet per second at the maximum-weight-flow operating point. At a wheel tip speed of 1184 feet per second the absolute Mach number near the hub (a radius of 5.36 in.) is 1.37; whereas near the tip (a radius of 6.96 in.) it decreases to 0.90.

As the flow is reduced while operating at constant speed, the absolute Mach number is reduced. At a wheel tip speed of 1036 feet per second and a radius of 6.06 inches (near the pitch radius), the absolute Mach number is reduced from a value of 0.94 at the maximum-flow point to a value of 0.88 at the incipient-stall point; whereas, at a wheel tip speed of 518 feet per second and a radius of 6.06 inches, the corresponding values are 0.52 and 0.47.

The radial distribution of absolute discharge angle (fig. 6(b)) is approximately the same for comparable operating points at wheel tip speeds of 622 and 829 feet per second in air. At higher speeds, the radial variation of absolute discharge angle increases for operation at the maximum-flow and maximum-efficiency points. For example, with operation at the maximum-flow points, the radial variation of absolute angle is approximately  $15^\circ$  at a wheel tip speed of 1036 feet per second and only about  $6^\circ$  at a wheel tip speed of 518 feet per second. The radial variation of absolute angle at the incipient-stall points is approximately the same for all speeds tested.

The radial distribution of total-pressure ratio is shown in figure 6(c). The maximum radial variation, which occurs at a wheel tip speed of 1184 feet per second, is from a value of 2.07 near the hub (radius of 5.66 in.) to a value of 1.72 near the tip (radius of 6.96 in.). The radial distribution of total-pressure ratio is approximately uniform at the lower wheel tip speeds.

#### Rotating Stall

At all speeds where stall data were taken, the rotating stall was an abrupt single-zone total-span stall which covered approximately one-third of the annulus area and always rotated in the direction of wheel rotation at a speed of approximately 77 percent of rotor speed.

#### Radial Distribution of Blade-Loading Characteristics

The diffusion factor (a blade-loading parameter for the minimum-loss-incidence-angle condition, derived in ref. 6) was used as an approximate measure of the blade loading. Figure 7 gives the variation of diffusion factor with weight flow at three radial locations.



It is noted that, at the incipient-stall points, the diffusion factor attains a value of 0.6 at the tip for all speeds (fig. 7(a)). At other radii (figs. 7(b) and (c)), the values at the incipient-stall points are less and vary with speed. Since the diffusion factor is greatest at the tip and is independent of speed, this blade-loading parameter indicates that the tip radius was the most critical. Also, the value of diffusion factor of 0.6 at the tip evidently was a limit for this rotor, but there is no reason to believe that this value has any significance for other compressors.

Furthermore, since at the incipient-stall points the largest incidence angle occurs at the tip at all speeds (fig. 5(b)), the tip section is the most critical in regard to incidence angle. It is thus believed that the stall begins at the tip and then instantaneously spreads across the entire span, thus giving an abrupt total-span stall.

Flow fluctuations. - The qualitative study of the flow fluctuations in the entrance and the exit with the hot-wire anemometers during stalled operation showed that the amplitude was large and of the approximate order of magnitude of the time-averaged value. The amplitudes of the fluctuations were approximately the same in the inlet and the exit and appeared relatively independent of speed and radius.

Pressure fluctuations. - The intensities of the static-pressure fluctuations on the casing, which were obtained from the catenary diaphragm pressure transducers, are shown in figure 8 for operating points during stalled operation near the incipient-stall point and stall-free operation at the maximum-flow point. When the impeller is operating in stall, the intensity of the pressure fluctuations in the inlet increase with increasing speed to large values, but the fluctuation intensity in the exit is negligible (fig. 8(a)). For example, at a wheel tip speed of 1036 feet per second, the root-mean-square fluctuation intensity at the inlet during stalled operation is approximately 12 percent of the time-averaged static pressure obtained from the static taps on the casing, whereas the peak-to-peak fluctuation intensity is 66 percent of the time-averaged static pressure. For stalled operation at a wheel tip speed of 1036 feet per second, the root-mean-square fluctuation intensity at the exit is 2 percent of the time-averaged static pressure, whereas the peak-to-peak value is 4 percent. The magnitude of these exit static-pressure fluctuations is approximately equal to the noise level of the pressure-transducer system.

During stall-free operation, the intensity of the pressure fluctuations is small at the exit and entrance except at a wheel tip speed of 1036 feet per second, where the fluctuations at the entrance become large (fig. 8(b)). The relative inlet Mach number at the tip became slightly supersonic at a wheel tip speed of 1036 feet per second (fig. 5(a)). The waves from the resulting pressure wave system travel upstream

and produce an unsteady pressure fluctuation ahead of the impeller (fig. 8(b)). As the speed is increased, these waves become contained by the blades, and the intensity of the pressure fluctuation decreases. The root-mean-square fluctuation intensity of these waves is 9.5 percent of the time-averaged static pressure; however, the peak-to-peak intensity is 33.6 percent of the time-averaged static pressure. At a wheel tip speed of 1184 feet per second, the root-mean-square fluctuation intensity in the entrance and exit is greater than the intensities at low speed because of unsteady conditions associated with flow at Mach numbers near sonic (see figs. 5(a) and 6(a)).

#### Evaluation of Weight-Flow Range

In order to determine the suitability of this high-solidity low-aspect-ratio transonic rotor with respect to range of weight flow, the range of this rotor was compared with that of the two transonic inlet stages of an eight-stage axial-flow compressor (refs. 7 and 8).

This eight-stage compressor when properly matched with a turbine could produce an engine with some weight-flow range available for acceleration. In the comparison of the weight-flow ranges, the best match point of the inlet stages of the eight-stage compressor was assumed to occur at a wheel tip speed of 1051 feet per second and an equivalent weight flow of 24.5 pounds per second per square foot of frontal area. The assumed match point of the high-solidity transonic rotor was at a wheel tip speed of 1036 feet per second and an equivalent weight flow of 24.3 pounds per second per square foot frontal area. A constant stator loss of 10 percent of the stator-inlet kinetic energy was assumed for the high-solidity transonic rotor. The stator was also assumed to impose no additional restriction on the range in weight flow of the high-solidity transonic rotor. The pressure ratio developed by the high-solidity transonic rotor (including the assumed stator losses), and the two transonic stages at their match points were very nearly the same (1.74 and 1.70, respectively). The transonic inlet stages and the high-solidity transonic rotor were compared on the basis of the dimensionless exit parameters,  $(w\sqrt{\theta_2/\delta_2})/(w\sqrt{\theta_2/\delta_2})_d$  and  $(U/\sqrt{\theta_2})/(U/\sqrt{\theta_2})_d$ , since the weight flow, the speed, and the state of the gas at the exit of the inlet stages must be the inlet conditions for the remainder of the compressor.

The most significant criterion for the evaluation of the stall-free weight-flow range of a stage would be one based on the range of weight flow between the compressor-stall line and the equilibrium operating line, since all weight-flow ranges at values higher than the equilibrium operating line are without significance. If it can be assumed that, when the high-solidity transonic rotor and the two transonic stages are each staged with comparable latter stages, the two compressors when used in engines would have identical engine equilibrium operating lines, the range in

weight flow of the high-solidity transonic rotor and the two transonic stages can be compared by comparing the first-stage stall lines. Figure 9 shows the stall-limit line of the high-solidity transonic rotor, the stall line of the inlet stages of the eight-stage compressor, and the stall-limit line of the eight-stage compressor. Since the high-solidity transonic rotor initiates stall at a higher percentage of design weight flow than the two transonic inlet stages, the cross-hatched area between the stall lines is a measure of the difference in stall-free range. For example, at a speed of 60 percent of design, the two transonic stages initiate stall at a corrected weight flow of 52.5 percent of design flow, while the high-solidity transonic rotor stalls at a flow of 62.5 percent of design flow. Thus, the high-solidity transonic rotor has less stall-free range than the two inlet transonic stages of the eight-stage compressor. Furthermore, because of the severity and radial extent of the flow fluctuations which persist throughout the high-solidity transonic rotor during stalled operation, it is doubtful whether this rotor could be staged with conventional stages and operate efficiently when the rotor is stalled.

#### Comparison of Performance of Unmodified and

#### High-Solidity Transonic Rotors

The removal of the inlet guide vanes and the cutting back of the blade trailing edge reduced the work input of this rotor and thus reduced the total-pressure ratio developed by the rotor. The total-pressure ratio was reduced approximately 20 percent from that developed by the unmodified rotor (ref. 4) for comparable wheel speeds.

The efficiencies of the unmodified and modified rotors were compared for several operating points of the two rotors. Comparable rotor operating points were obtained by selecting from the data those pairs of conditions for which the relative inflow directions to the rotors were the same and for which the inflow relative Mach numbers were equal. (Comparable rotor operating points, therefore, did not occur at the same wheel tip speeds.) Because the hub-to-tip conditions varied differently, it was only possible to match using average conditions. The adiabatic efficiencies of the unmodified rotor (ref. 4) were approximately equal to those of the high-solidity transonic rotor during stalled operation. Since the efficiencies were approximately equal, it might be suspected that some type of stall or surge was present over the entire range of flow of the unmodified rotor. However, the unsteady flow was not studied at comparable wheel tip speeds in the unmodified rotor to substantiate the presence of stall or surge. Surge was not encountered at any speed in the modified high-solidity transonic rotor.

## Stator Problems

Average discharge Mach number and angle. - The mass-averaged absolute discharge Mach number is plotted against the mass-averaged absolute discharge angle in figure 10. The absolute discharge angle varies only  $3^\circ$  as the speed is increased while operating at points of maximum rotor efficiency. The absolute discharge angle varies only  $12^\circ$  over the entire stall-free range of weight flow. This small variation in the absolute discharge angle over the weight-flow range is due to the small stall-free range of weight flow. Since the absolute discharge angle is directly related to the stator incidence angle, the range of stator incidence angle would also be  $12^\circ$ .

Stator design incidence angle. - Compressor tests involving double-circular-arc blades (ref. 9) show that, at inlet Mach numbers of 0.8 or higher, the incidence angle is a critical factor in attaining efficient flow. At lower inlet Mach numbers (ref. 9), efficient flow can be attained over a wide range of incidence angles. Since the absolute discharge Mach number from the rotor is high subsonic at high speeds (fig. 10), judicious selection of the design incidence angles is necessary for the attainment of efficient flow. At lower speeds the rotor discharge Mach number is reduced, and therefore efficient flow can be attained over an appreciably larger range of incidence angles or range of weight flows.

Radial variations of angle, Mach number, and pressure ratio. - The radial variation of absolute discharge angle, absolute discharge Mach number, and total-pressure ratio at the entrance to the stator are given in figure 6. The radial distribution of absolute discharge Mach number is quite uniform at all speeds except 1184 feet per second (fig. 6(a)), where the absolute discharge Mach number varies from approximately 0.9 at the tip to 1.3 at the hub.

The maximum radial variation of absolute angle is  $18.5^\circ$  and occurs at a wheel tip speed of 1184 feet per second at the maximum-weight-flow conditions (fig. 6(b)). The maximum radial variation in absolute angle at the maximum-efficiency operating points is  $10^\circ$  and occurs at a wheel speed of 1036 feet per second (fig. 6(b)). The radial variation of absolute angle at incipient-stall points is approximately  $11^\circ$  for all speeds.

There are no large radial gradients of the total-pressure ratio (fig. 6(c)). Therefore, one of the stator problems is eliminated; that is, the problem of stator mixing losses.

Stator blade vibrations. - Since the rotor has a span of only 1.84 inches at the exit, the stators would have an aspect ratio of the order of those found in the exit stages of multistage axial-flow compressors and would have a high resonant frequency. Therefore, no serious blade vibrations due to resonance during stalled operation would be expected.

3737

CB-2 back

## SUMMARY OF RESULTS

A high-solidity low-aspect-ratio transonic rotor with an inlet hub-tip radius ratio of 0.52 was tested, and the performance was analyzed with regard to its suitability as an inlet stage of a multistage compressor. A rotor with a low aspect ratio can be expected to be rugged and free of blade vibration problems. Results of the tests and analyses are as follows:

1. The rotor developed an efficiency of 92 percent and a total-pressure ratio of 1.93 at an equivalent wheel tip speed of 1036 feet per second. At all lower speeds, the peak efficiency remained above 90 percent.

2. At all speeds an abrupt total-span rotating stall was observed, which consisted of one stalled region rotating at approximately 77 percent of wheel speed. The stalled region covered approximately one-third of the annulus area.

3. Blade stall occurred over the whole blade span but was initiated at the tip because of the higher incidence angle and the greater diffusion required. For all speeds, stall occurred when the diffusion factor reached 0.6 at the tip of the blades.

4. Qualitative results from hot-wire anemometers during stalled operation indicate that the amplitude of the flow fluctuations are of the approximate order of magnitudes of 100 percent of the time-averaged value of flow. The amplitude is approximately the same in the inlet and exit and appears relatively independent of speed.

5. During operation with rotating stall, the static-pressure fluctuations at the casing are large in the inlet and increase with increases in speed. At a wheel tip speed of 1036 feet per second, the root-mean-square fluctuation intensity and the peak-to-peak fluctuation intensity during stalled operation are 12 percent and 66 percent of the time-averaged static pressure, respectively. The pressure fluctuations in the exit are negligible.

During stall-free operation, the static-pressure fluctuations in the inlet and exit are small except at a wheel tip speed of 1036 feet per second, where waves, which arise from the pressure-wave system at the tip radius, travel upstream.

6. A comparison of the weight-flow range of this high-solidity transonic rotor with that of the two transonic stages used in an eight-stage

high-pressure-ratio axial-flow compressor revealed that the stall-free weight-flow range of the transonic stages was larger than that of this high-solidity transonic rotor.

Lewis Flight Propulsion Laboratory  
National Advisory Committee for Aeronautics  
Cleveland, Ohio, September 19, 1955

#### REFERENCES

1. Delio, G. J., and Stiglic, P. M.: Experimental Investigation of Control Signals and the Nature of Stall and Surge Behavior in a Turbojet Engine. NACA RM E54I15, 1954.
2. Huppert, Merle C., and Benser, William A.: Some Stall and Surge Phenomena in Axial-Flow Compressors. Jour. Aero. Sci., vol. 20, no. 12, Dec. 1953, pp. 835-845.
3. Herrig, L. Joseph, Emery, James C., and Erwin, John R.: Systematic Two-Dimensional Cascade Tests of NACA 65-Series Compressor Blades at Low Speeds. NACA RM L51G31, 1951.
4. Schacht, Ralph L., Goldstein, Arthur W., and Neumann, Harvey E.: Performance of a Supersonic Rotor Having High Mass Flow. NACA RM E54D22, 1954.
5. Bullock, Robert O., Wilcox, Ward W., and Moses, Jason J.: Experimental and Theoretical Studies of Surging in Continuous-Flow Compressors. NACA Rep. 861, 1946. (Supersedes NACA TN 1213.)
6. Lieblein, Seymour, Schwenk, Francis C., and Broderick, Robert L.: Diffusion Factor for Estimating Losses and Limiting Blade Loading in Axial-Flow-Compressor Blade Elements. NACA RM E53D01, 1953.
7. Voit, Charles H., and Geye, Richard P.: Investigation of a High-Pressure-Ratio Eight-Stage Axial-Flow Research Compressor with Two Transonic Inlet Stages. III - Individual Stage Performance Characteristics. NACA RM E54H17, 1954.
8. Geye, Richard P., Budinger, Ray E., and Voit, Charles H.: Investigation of a High-Pressure-Ratio Eight-Stage Axial-Flow Research Compressor with Two Transonic Inlet Stages. II - Preliminary Analysis of Over-All Performance. NACA RM E53J06, 1953.

9. Schwenk, Francis C., Lieblein, Seymour, and Lewis, George W., Jr.:  
Experimental Investigation of an Axial-Flow Compressor Inlet Stage  
Operating at Transonic Relative Inlet Mach Numbers. III - Blade-  
Row Performance of Stage with Transonic Rotor and Subsonic Stator  
at Corrected Tip Speeds of 800 and 1000 Feet Per Second. NACA RM  
E53G17, 1953.

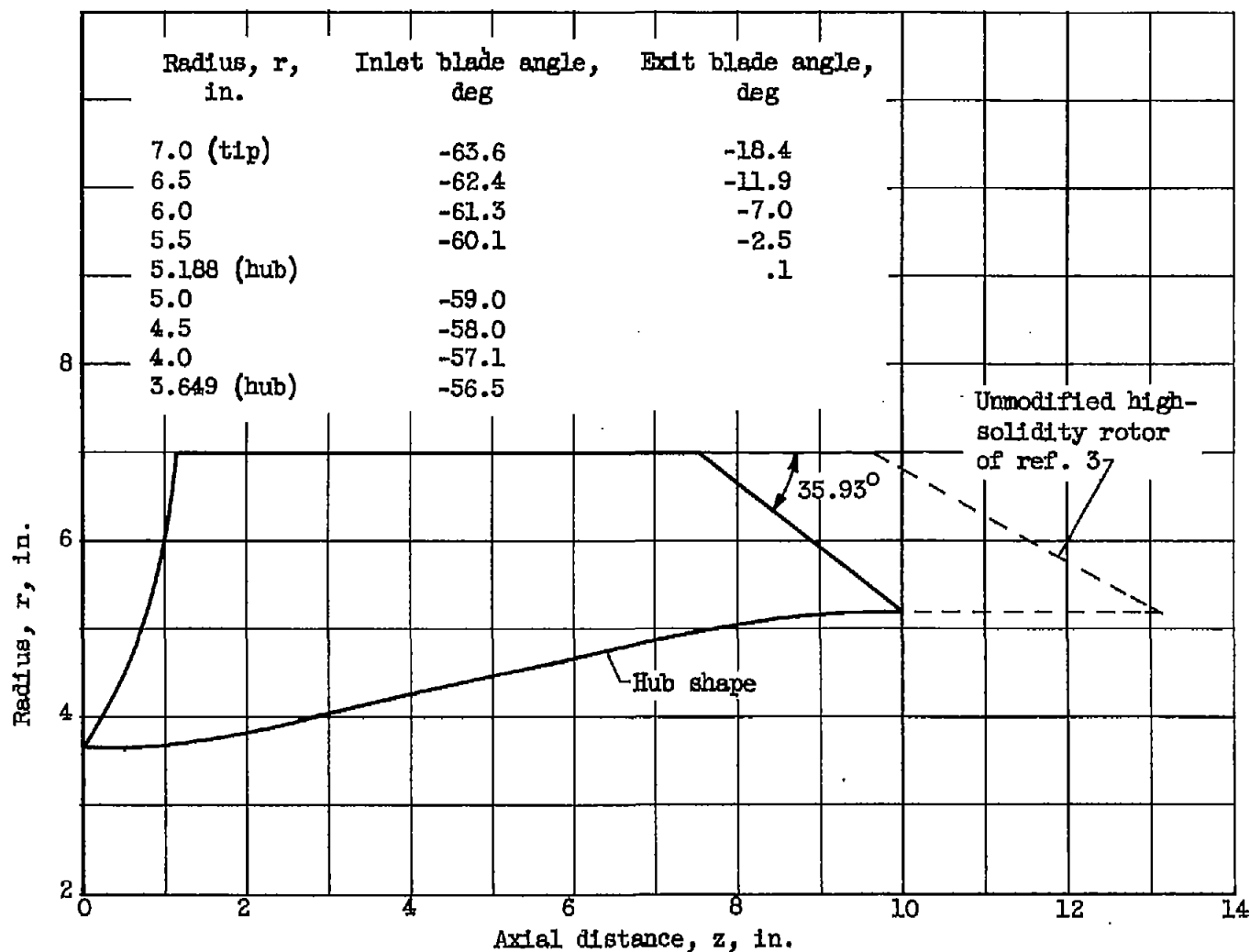
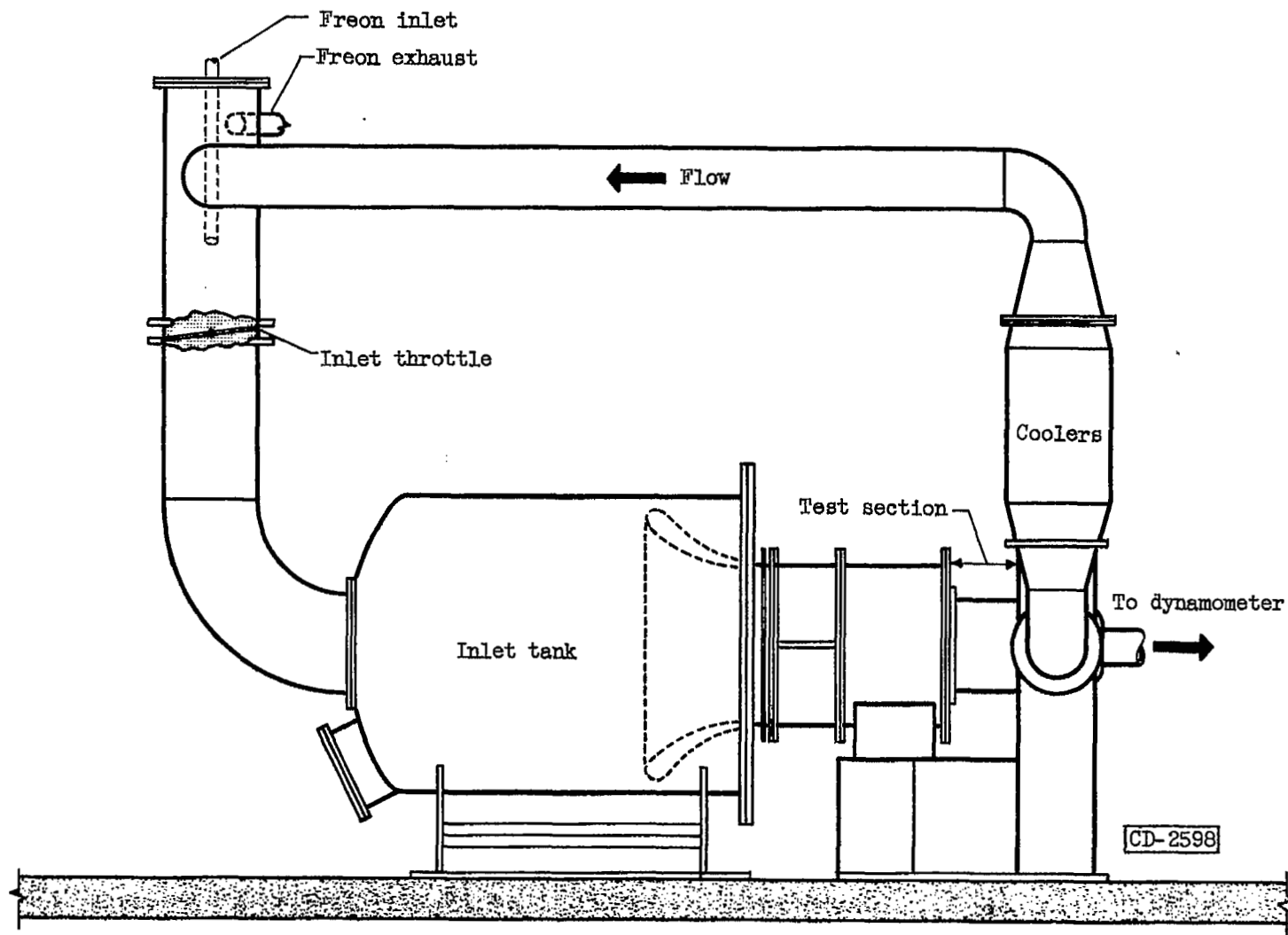


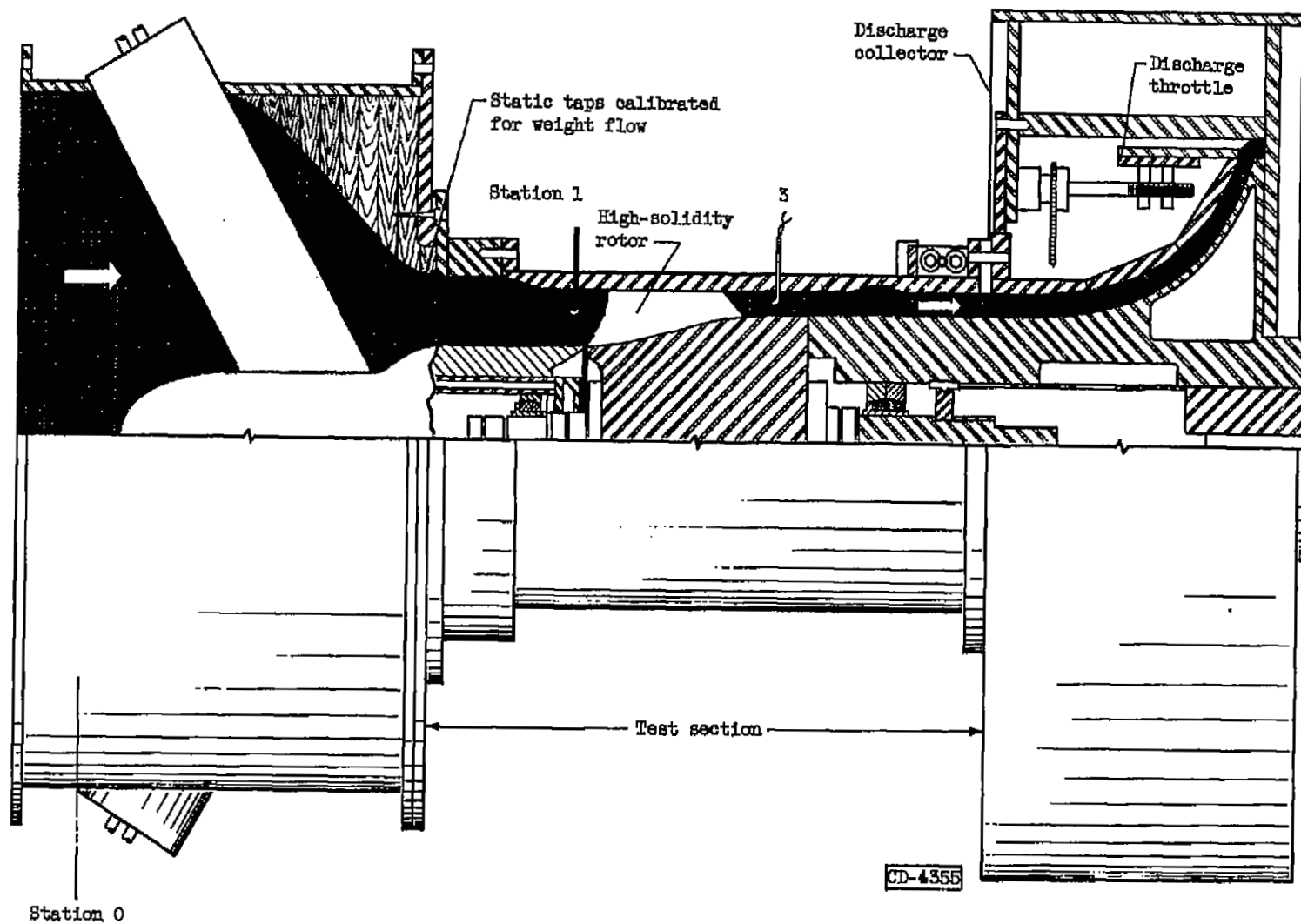
Figure 1. - Inlet and exit blade angles and schematic sketch of modification made to obtain 14-inch high-solidity low-aspect-ratio transonic rotor.





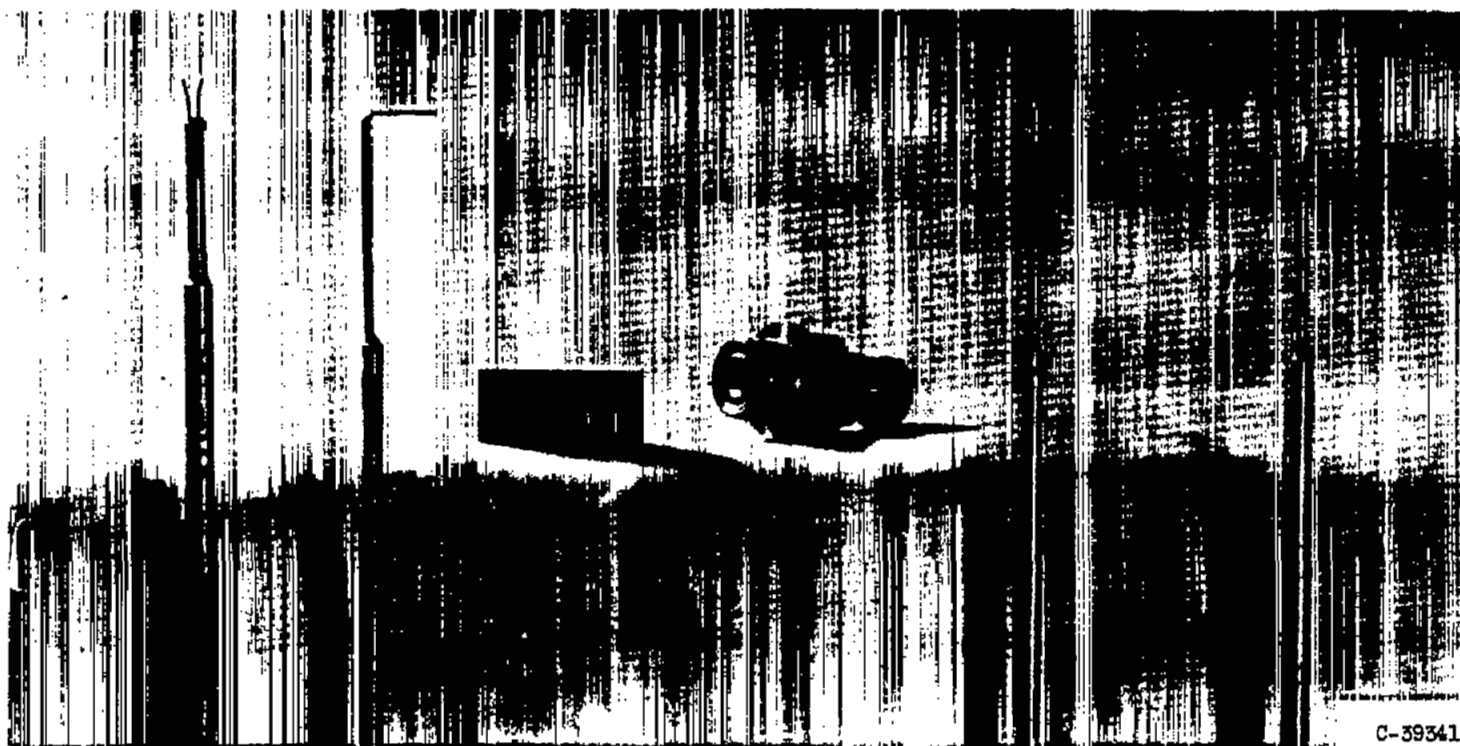
(a) Piping assembly.

Figure 2. - Schematic diagram of compressor installation.



(b) Test section.

Figure 2. - Concluded. Schematic diagram of compressor installation.



C-39341

(a) Hot-wire-  
anemometer probe.

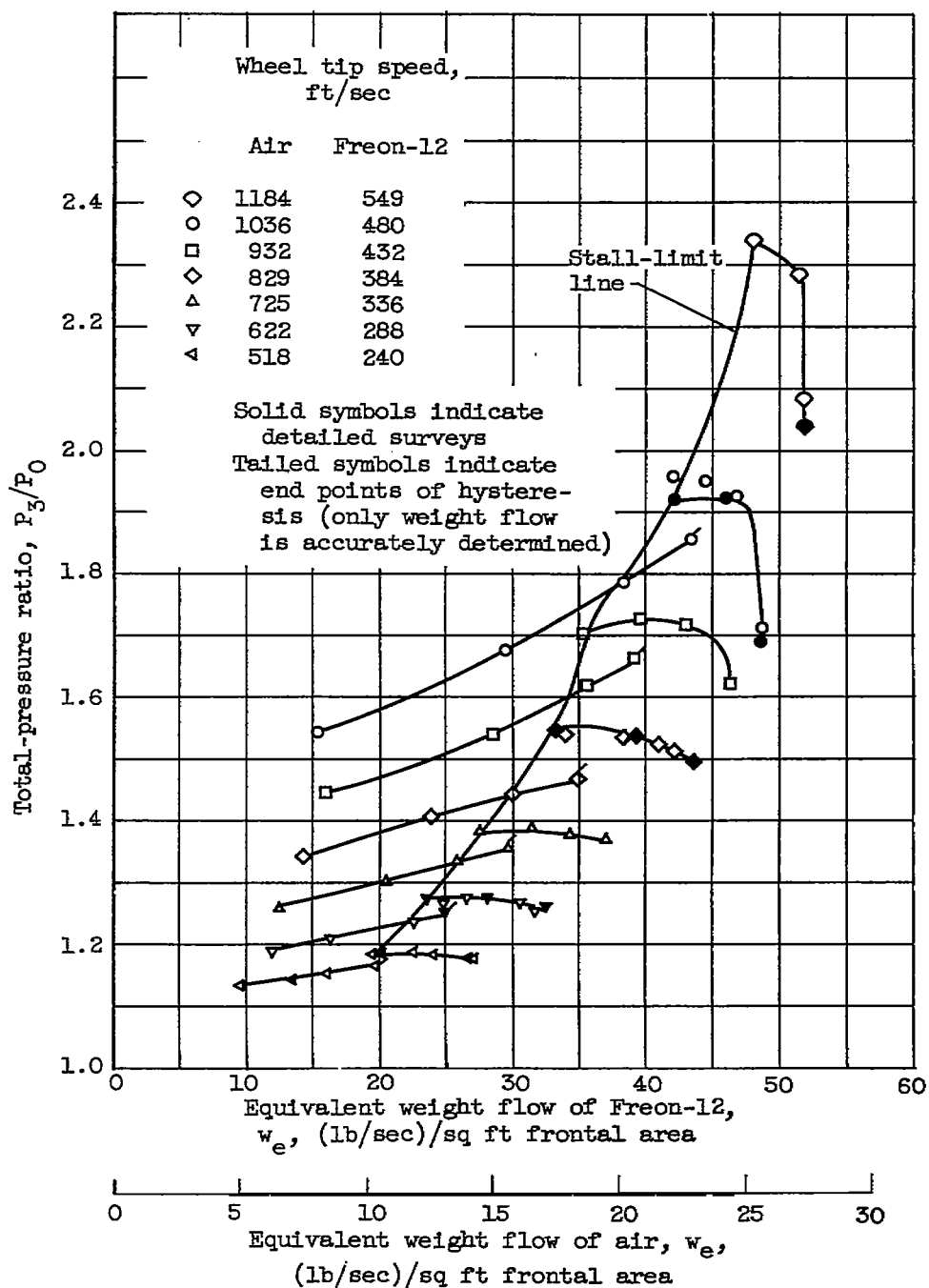
(b) L static-  
pressure probe.

(c) Pressure  
transducer.

(d) Total-temperature  
probe.

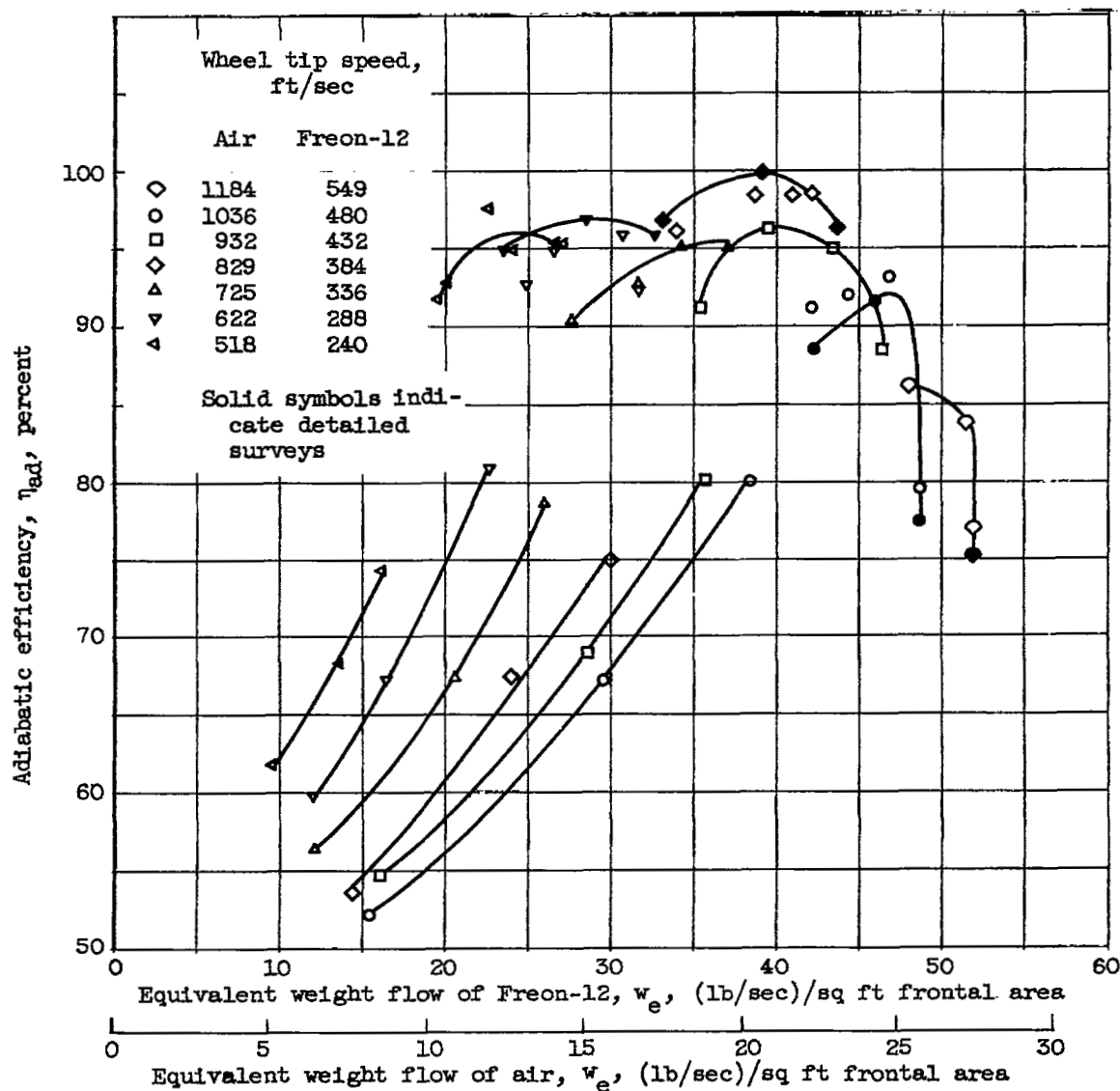
(e) Claw - total-  
pressure probe.

Figure 3. - Typical probes and pressure transducer used to determine performance characteristics of 14-inch high-solidity low-aspect-ratio transonic rotor.



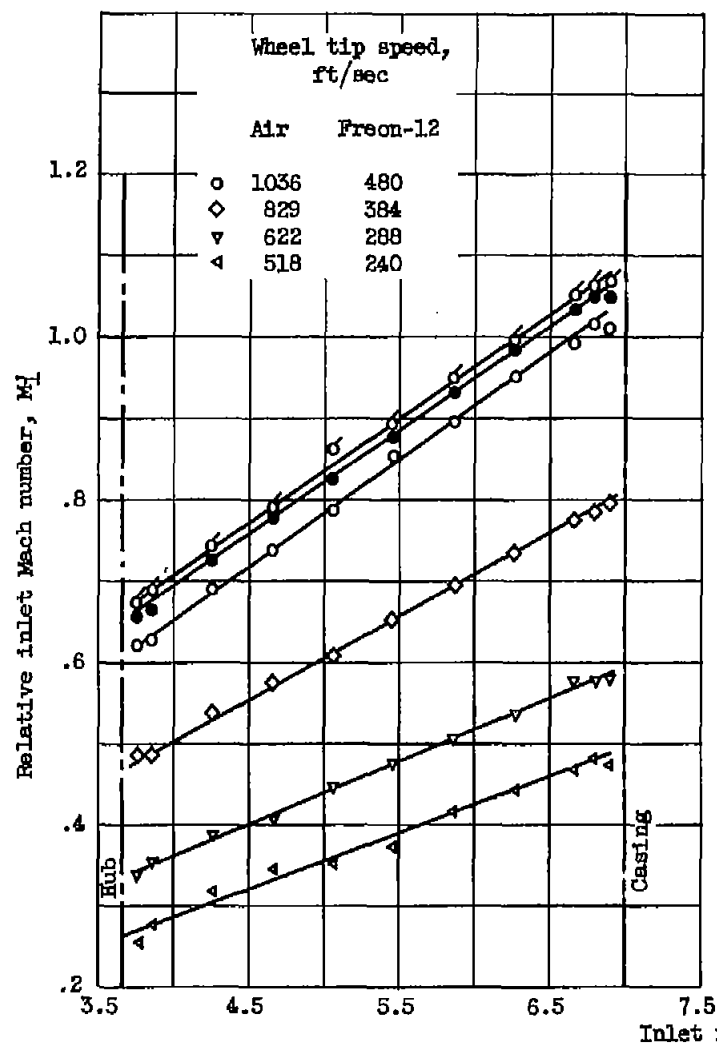
(a) Total-pressure ratio.

Figure 4. - Over-all performance characteristics of high-solidity transonic rotor.

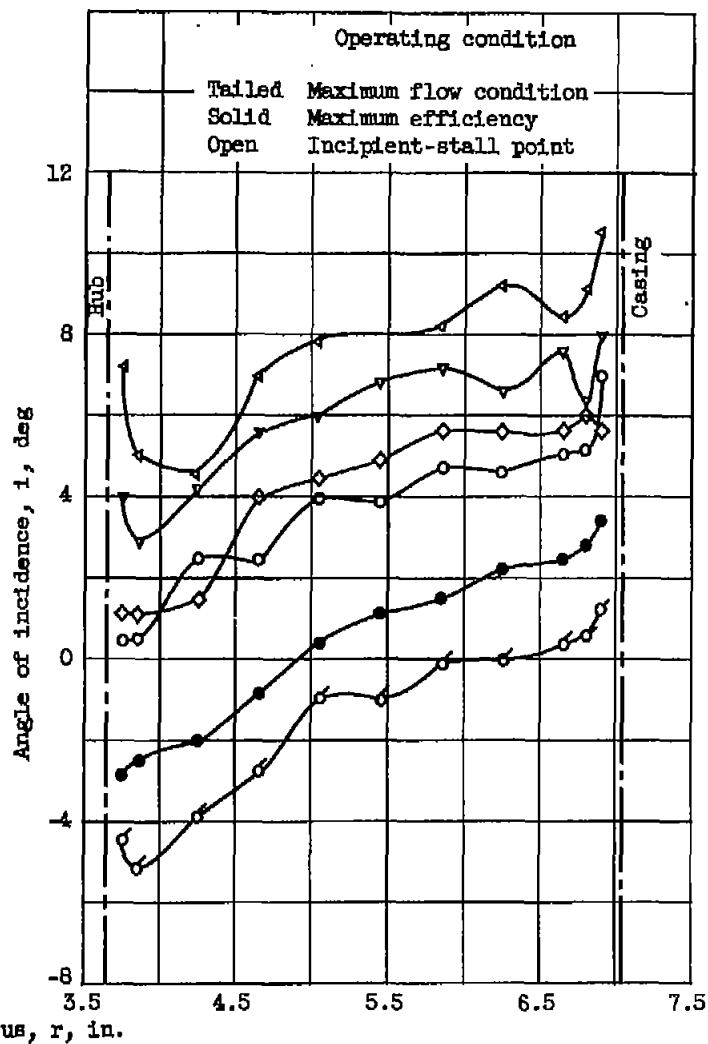


(b) Adiabatic efficiency.

Figure 4. - Concluded. Over-all performance characteristics of high-solidity transonic rotor.

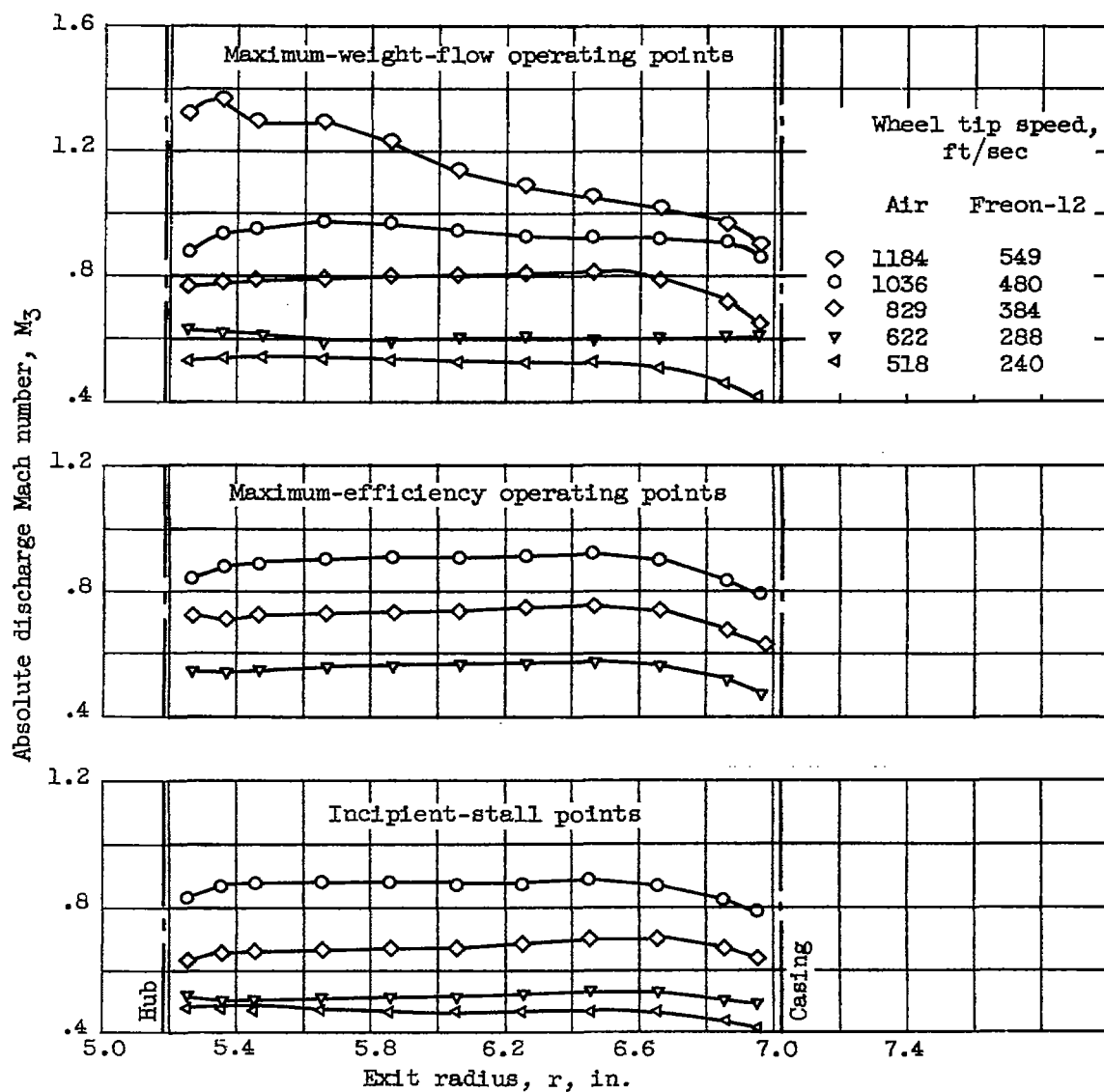


(a) Relative Mach number.



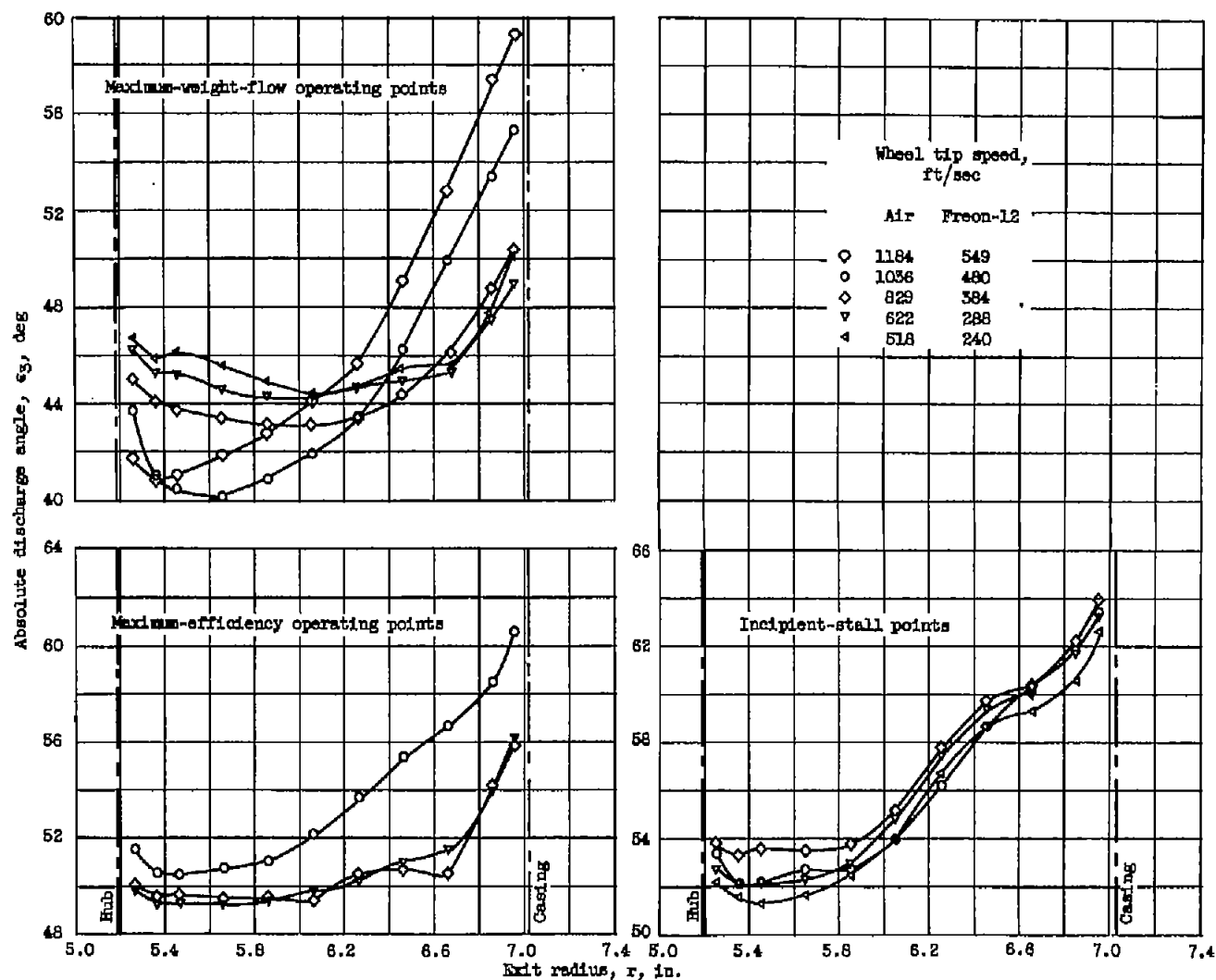
(b) Incidence angle.

Figure 5. - Radial distribution of relative inlet Mach number and incidence angle for 14-inch high-solidity low-aspect-ratio transonic rotor.



(a) Radial variations of absolute discharge Mach number.

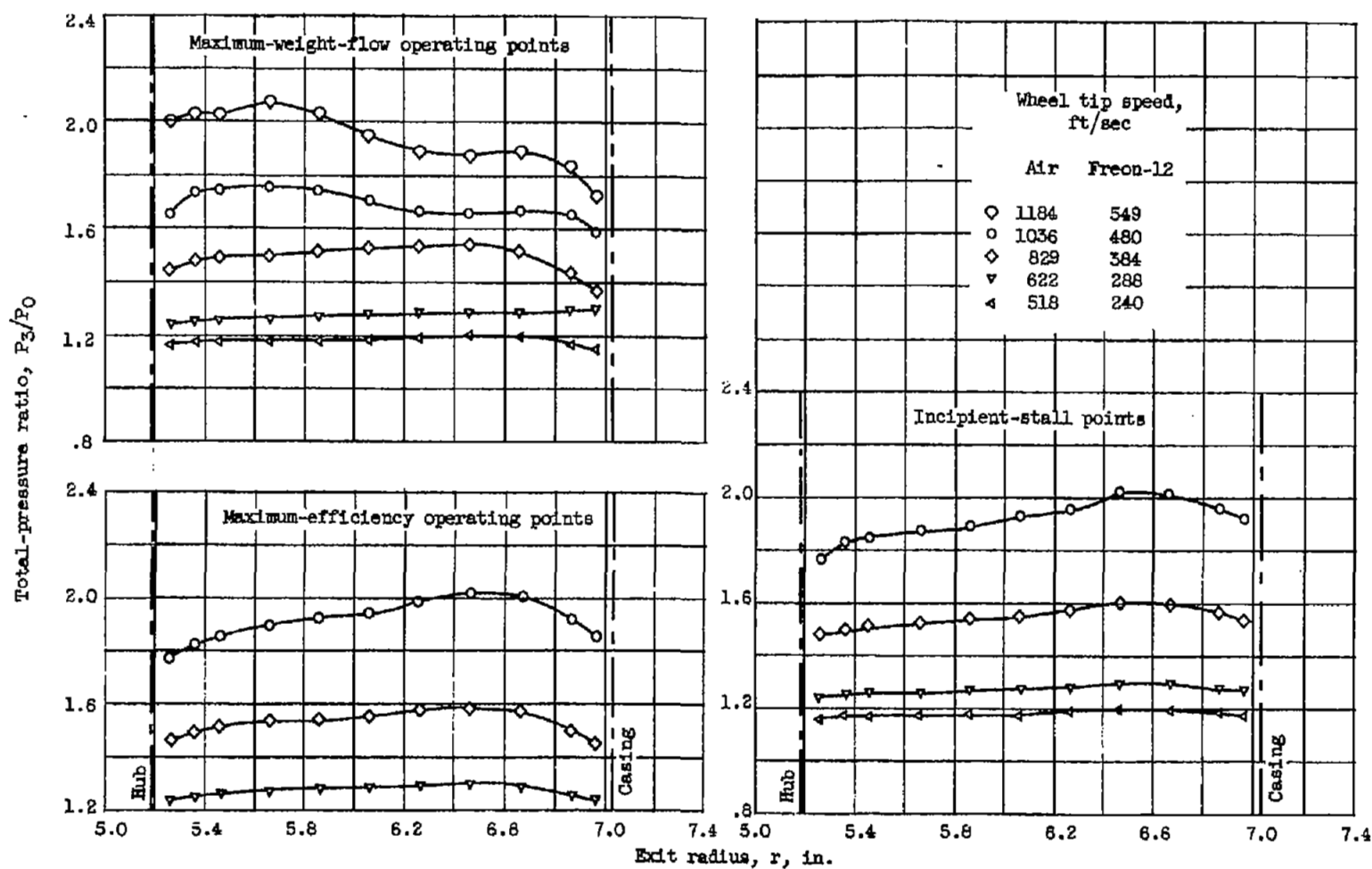
Figure 6. - Conditions at rotor discharge for various speeds.



(b) Radial variations of absolute discharge angle.

Figure 6. - Continued. Conditions at rotor discharge for various speeds.





(c) Radial variations of total-pressure ratio.

Figure 6. - Concluded. Conditions at rotor discharge for various speeds.

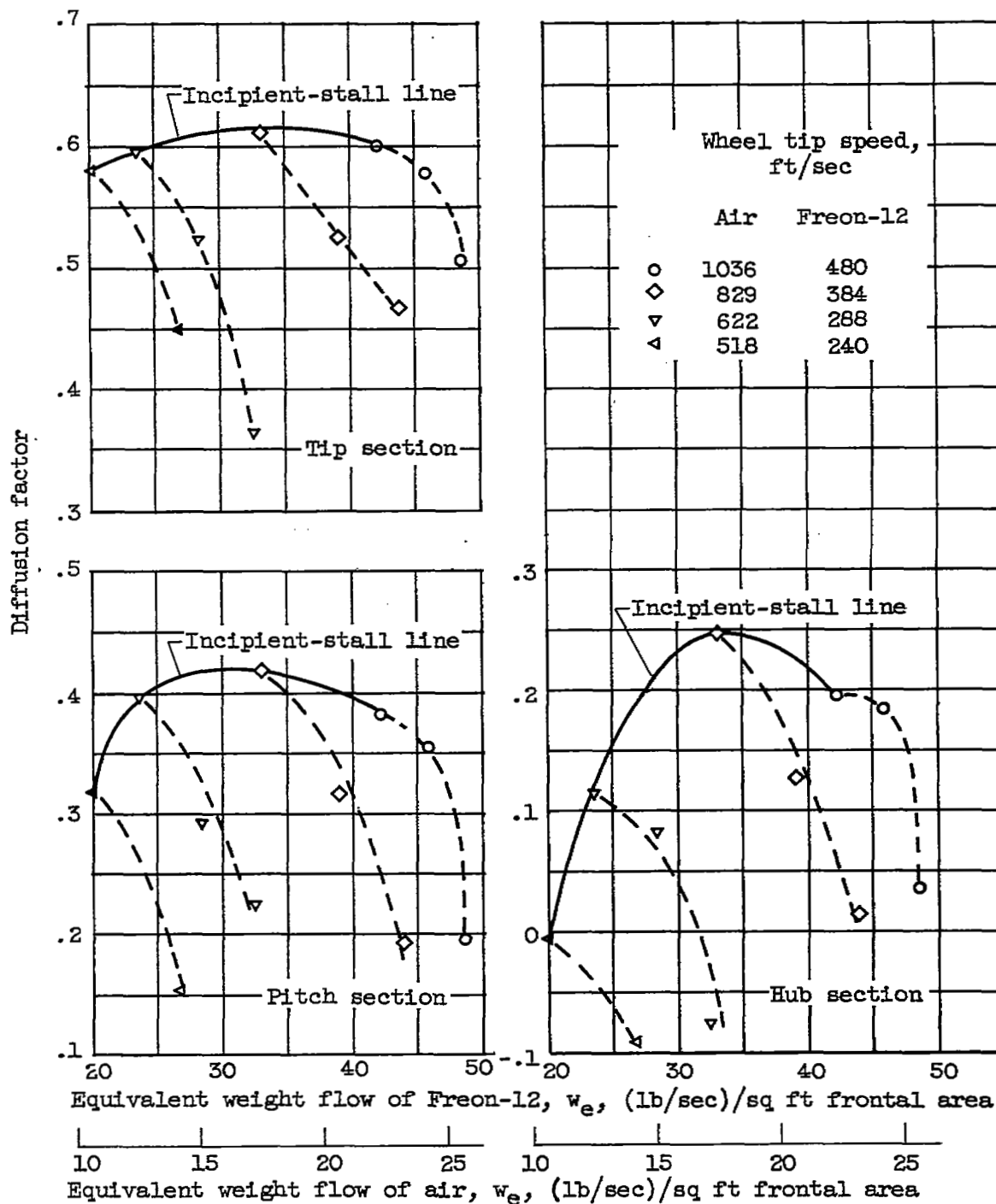
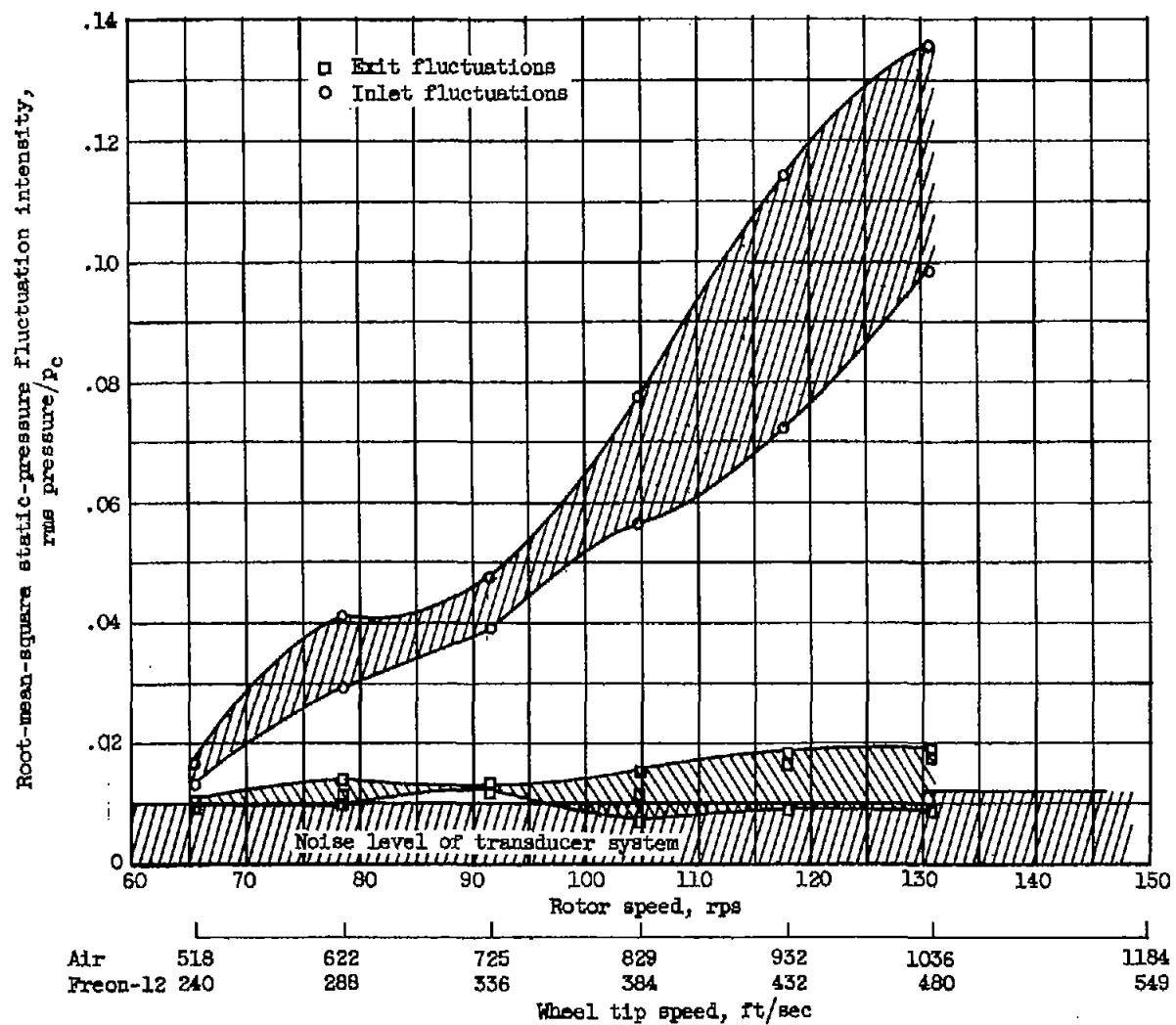
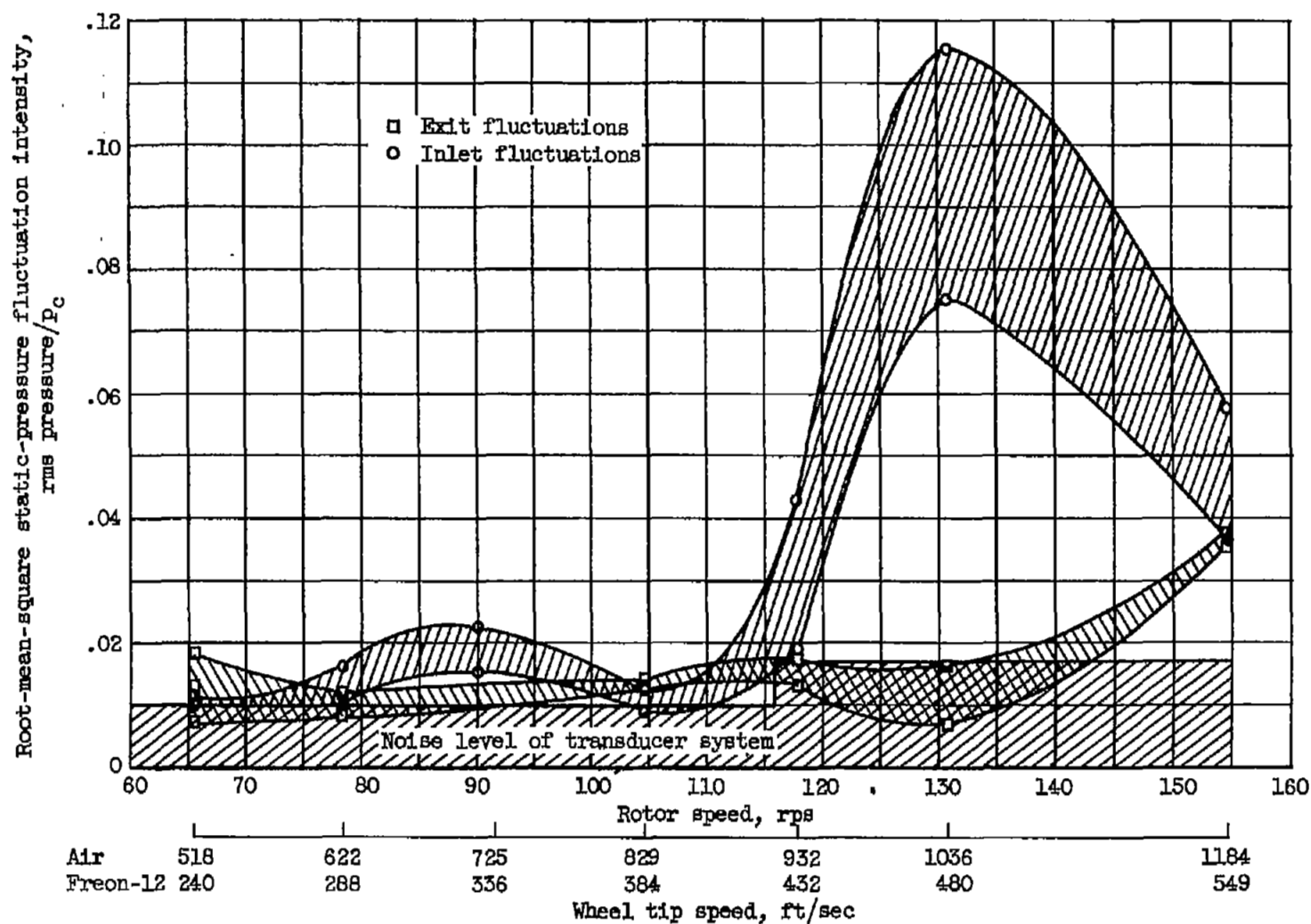


Figure 7. - Variation in diffusion factor with weight flow during stall-free operation.



(a) During rotating stall.

Figure 8. - Inlet and exit static-pressure fluctuations on casing.



(b) During stall-free operation.

Figure 8. - Concluded. Inlet and exit static-pressure fluctuations on casing.

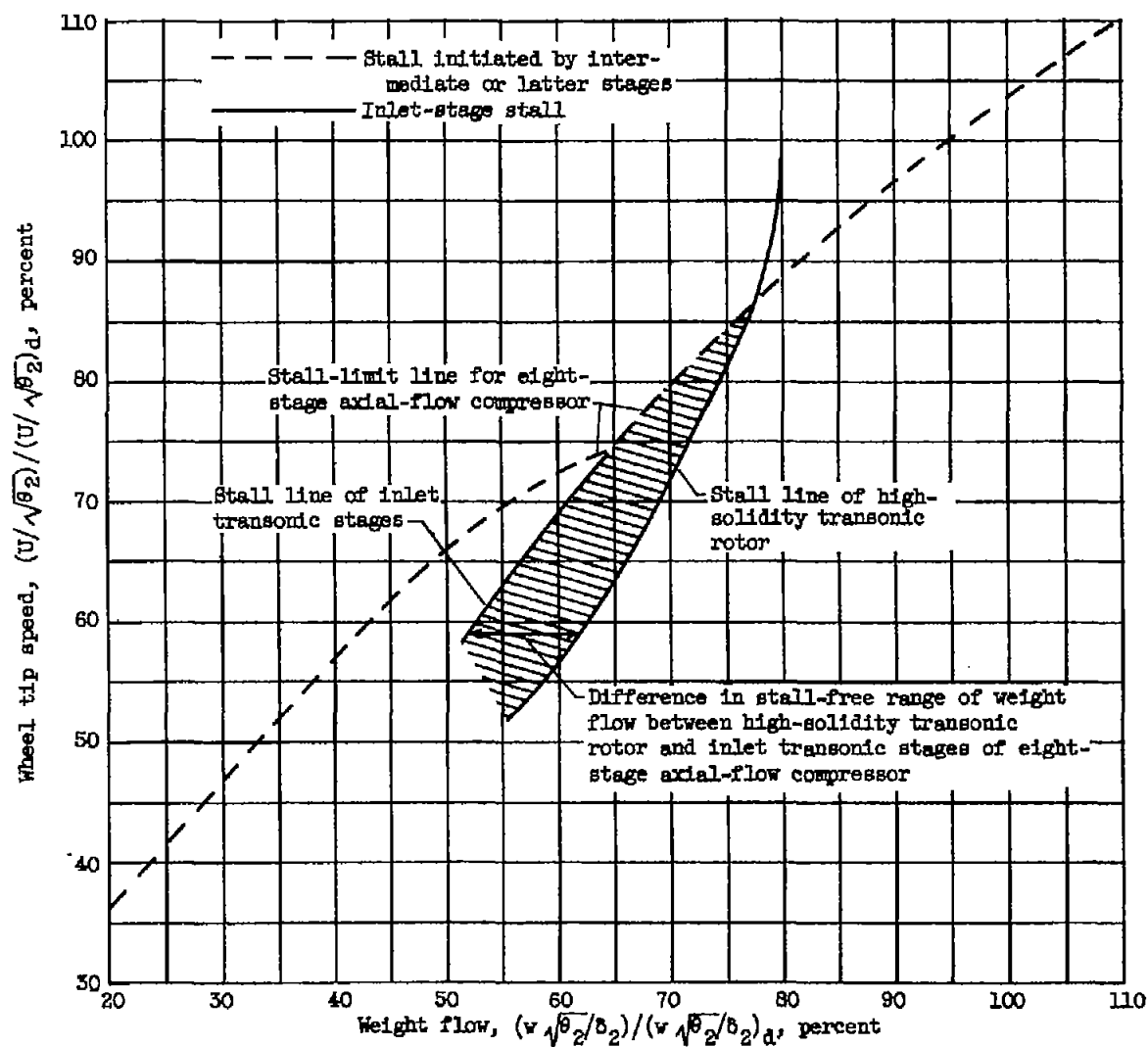


Figure 9. - Comparison of stall lines of 14-inch high-solidity transonic rotor and eight-stage axial-flow compressor.

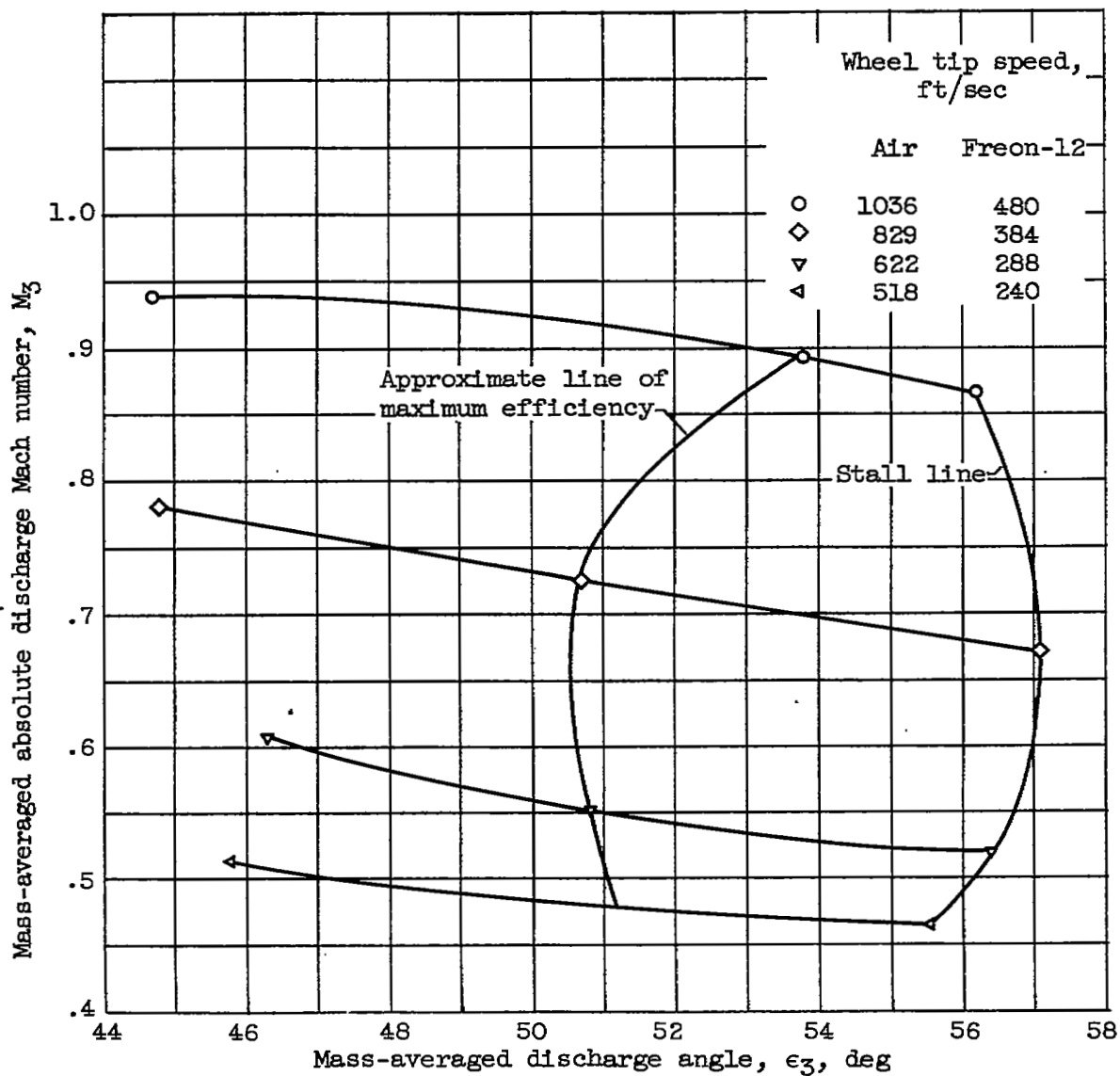


Figure 10. - Variation of mass-averaged absolute discharge angle with mass-averaged absolute discharge Mach number.

NASA Technical Library



3 1176 01436 5242

